Engineering Structures 128 (2016) 184–198

Contents lists available at ScienceDirect

Engineering Structures

journal homepage: www.elsevier.com/locate/engstruct

The enhanced performance of CFST beams using different strengthening schemes involving unidirectional CFRP sheets: An experimental study

Ahmed W. Al Zand *, Wan Hamidon W. Badaruzzaman, Azrul A. Mutalib, Salam J. Hilo

Department of Civil and Structural Engineering, Universiti Kebangsaan Malaysia, 43600 Bangi, Selangor, Malaysia

ARTICLE INFO

Article history:
Received 2 June 2016
Revised 21 September 2016
Accepted 21 September 2016
Available online 28 September 2016

Keywords:
CFST beam
Flexural stiffness
Partial strengthening scheme
CFRP sheets

ABSTRACT

Concrete-filled steel tube (CFST) beam, like any conventional structural member, for several reasons need strengthening, such as by making upgrades to carry extra loads or to make repairs owing to degradation attributed to aging, fire, and fatigue. This study experimentally investigates the strengthening behaviour of the circular and rectangular simply supported CFST beams using unidirectional carbon fibre reinforced polymer (CFRP) sheets, in which partial-unilateral (partial), full-unilateral (full), and full-bilateral (combined) strengthening schemes with varied layers and lengths are used. The results show that the moment capacity, energy absorption capacity, and flexural stiffness of the strengthened beam significantly improved with the increase of CFRP layers. For example, the moment capacity of the rectangular beams increased by about 26% and 38% when they were partially strengthened with two and three CFRP layers, respectively. Also, the beams were partially strengthened with two CFRP layers laid along 75% and 100% of their lengths, and that fully strengthened along 100% of its length, all achieved almost the same load improvements (+26% to +28%) in comparison with their control beam, which means that about 50% of the amount of CFRP sheets or even more can be saved and the same improvement can be achieved. The energy absorption capacity of the circular beams improved by about 21.8% when they were partially strengthened with two CFRP sheets, for example. Moreover, the flexural stiffness values of the strengthened beams fairly agreed with those predicted from the existing standards (AISC, EC4, BS5400, and AIJ) after including the effects of CFRP.

1. Introduction

In recent times, engineers have increasingly utilized composite members of concrete-filled steel tubes (CFSTs) in modern projects such as buildings and bridges [1,2]. These types of composite structural members (CFSTs) have proven to be stronger and more ductile than the conventional steel tube members with equivalent shapes and material properties, as presented in [3,4]. This is because the concrete infill can prevent or delay the local buckling of the tube's wall, which usually happens in the high-compression zones of the hollow members [1]. Moreover, the CFST members are more economical and allow for rapid construction and cost savings by eliminating formwork and workmanship [5].

Like other structural members, CFST members may require strengthening for different reasons. For instance, they may require upgrading so that they can carry extra loads and/or they may need to be repaired due to degradation attributable to aging, fire, and fatigue. In the last few years, several research studies have been undertaken to determine the efficiency of using fibre-reinforced polymer (FRP) to strengthen steel members. They have looked into the use of different strengthening techniques, the application of loads, and bonding behaviour between the steel surfaces and the FRP materials [6]. One of the popular types of FRP is the carbon fibre-reinforced polymer (CFRP) fabric sheet, which has high tensile strength and a high modulus of elasticity compared to steel, is easy to handle, and is very flexible (it can be formed into structural members of any shape) [5,6]. Several experimental studies have proved the validity of using the CFRP sheets to retrofit and repair the compression of CFST members subjected to axial and/or axial-bending (combined) loads, such as given in [7–15]. Meanwhile, few studies have investigated the effects of using CFRP sheets to strengthen CFST beams which have been subjected to pure static bending loads [5,16–20].

Furthermore, the strengthening behaviour of hollow steel tube beams using circumferential CFRP wrapping schemes (that have fully wrapped the beams' cross-sections) was investigated earlier in several studies such as given in [21,22]. Also, this full wrapping scheme (circumferential) has been used to strengthen CFST beams [5,18–20]. In general, the behaviour and capacities of the simply

* Corresponding author.
E-mail address: ahmedzand70@gmail.com (A.W. Al Zand).

http://dx.doi.org/10.1016/j.engstruct.2016.09.044
0141-0296/

Nomenclature

A_s	area of steel tube cross-section (mm^2)
A_c	area of concrete core cross-section (mm^2)
B	width of rectangular steel tube (mm)
CFRP	carbon fibre reinforced polymer
CFST	concrete-filled steel tube
C	combined strengthening scheme
D	diameter of circular steel tube/depth of rectangular steel tube (mm)
EA	energy absorption (kN.mm)
E_c	concrete modulus of elasticity (GPa)
E_s	steel modulus of elasticity (GPa)
$E_{cfrp,patch}$	CFRP patch modulus of elasticity (GPa)
$E_{cfrp.sheet}$	CFRP sheet modulus of elasticity (GPa)
E_{ad}	adhesive modulus of elasticity (GPa)
f_{cu}	concrete cube compressive strength (MPa)
f_c	concrete cylinder compressive strength (MPa)
f_{ck}	characteristic concrete strength (MPa)
f_y	yield strength of steel (MPa)
f_u	ultimate strength of steel (MPa)
FRP	fibre reinforced polymer
F	full strengthening scheme
I_s	moment of inertia for steel tube cross-section (mm^4)
I_c	moment of inertia for concrete core cross-section (mm^4)
$I_{cfrp.patch}$	moment of inertia for CFRP patch (mm^4)
K_{ie}	initial flexural stiffness of composite section (experimental) ($kN.m^2$)
K_{se}	serviceability-level flexural stiffness of composite section (experimental) ($kN.m^2$)
K_p	predicted flexural stiffness of composite section (steel and concrete) ($kN.m^2$)
K_{cfrp}	predicted flexural stiffness of CFRP patch only ($kN.m^2$)
K_t	total flexural stiffness of composite section (steel, concrete and CFRP) ($kN.m^2$)
L	CFRP layers applied on CFST beam
LIR	load improvement ratio
L_e	effective length of specimen (support-to-support) (mm)
L_{CFRP}	length of CFRP sheets applied along the specimen (mm)
M	bending moment (kN.m)
M_{ue}	ultimate bending moment capacity (moment carrying capacity) (kN.m)
n	number of CFRP layers, used in the theoretical calculation of K_{cfrp}
P	partial strengthening scheme
t	wall thickness of steel tube (mm)
$t_{cfrp.patch}$	equivalent thickness of each CFRP patch (mm)
$t_{cfrp.sheet}$	thickness of each layer of CFRP sheet (mm)
t_{ad}	thickness of each adhesive layer (mm)
φ	curvature (1/m)

supported steel I-beams improve significantly when strengthened with unidirectional CFRP sheets laid parallel to them along the bottom flange only (tension flange) [23–25], taking advantage of these unidirectional sheets' capacity to sufficiently resist the high-tension stress. Following the above I-beam strengthening concept, strengthening the simply supported CFST beams on the bottom-half of their cross-sections (tension zones) alone with the unidirectional CFRP sheets could be considered a sufficient solution as well. Also, it could be difficult to fully wrap the beams' cross-sections, specifically when the CFST beams are used in the floor/roof system [2] or as the main girder for bridges [1], since the loads are usually applied on the top side (top flanges of the beams).

To date, very few studies have investigated the behaviour of these CFST beams using the partial CFRP strengthening scheme, by which the CFRP sheets have been applied along just the bottom flanges [16] and/or along the bottom-half of the beams' cross-sections [17]. For example, in 2013, Sundarraja and Ganesh [17] investigated the effects of three strengthening schemes of unidirectional CFRP sheets in the upgrading of square CFST beams. They used a flat scheme (the fibres were bonded along the entire length of just the bottom flange of the beam) and a U-shaped scheme (the fibres were bonded along the entire bottom-half of the beam's cross-section). Additionally, they used a third scheme, which was also flat but applied along part of the beam's length (the distance between the two loading points). For the three schemes, the CFRP fibres' orientation was parallel to the beams' lengths. The beams with the U-shaped scheme showed better load-improvement ratios than those with the flat strengthening scheme, whereas the beams with the partial flat strengthening scheme did not show much load improvement due to the CFRP delamination failure.

Therefore, the main aim of this study is to investigate the influence of unidirectional CFRP sheets when they are laid parallel to simply supported CFST beams using the following strengthening schemes: the partial-unilateral (partial), full-unilateral (full), and full-bilateral (combined) strengthening schemes. Fourteen specimens were tested experimentally using pure static bending loads (four-point bending). They included eight specimens with rectangular cross-sections and six specimens with circular cross-sections. This paper discusses the failure modes, moment capacities, energy absorption, and stiffness of the beams as indicated in the test results. The strengthened specimens' flexural stiffness values, as indicated in the test results, are compared with those predicted from different code standards after included the effects of CFRP sheets, where the stiffness value of the CFRP patch estimated theoretically using new concept has not been adopted before.

2. Experimental work

2.1. Material properties

Rectangular and circular cross-sections of hollow steel tubes were used for the CFST beams. For each tube's shape, three coupons were cut and prepared in accordance with ASTM-E8/8 M [26] for the tensile test. Table 1 presents the steel tubes' properties, which were obtained by testing the coupons (the average results of the three coupons for each tube shape).

The concrete-mix components were designed to achieve a compressive strength of 25 MPa. Two concrete batches were used to cast each group of steel tubes according to cross-section type. The average compressive strength of three cubes at 28 days was 31.5 MPa and 30.2 MPa for the rectangular and circular CFST specimens, respectively.

The type of unidirectional CFRP fabric sheet used in this study was the SikaWrap-231C. Three flat coupons were prepared in accordance with ASTM-D3039 [27] to determine the actual tensile strength. The adhesive material, Sikadur-330, was used as epoxy material to bond the CFRP sheets with the steel tubes and with the multiple layers of sheets. This adhesive material was a mix of two parts of resin (A) and hardener (B) with a ratio of 4:1 by weight. Table 2 presents the physical properties of the adhesive material and the CFRP sheets, which were obtained from the cou-

Table 1
Material properties of rectangular and circular steel tubes.

Tube's cross-section	D × B × t (mm) *or* D × t (mm)	Yield Strength f_y (MPa)	Ultimate strength f_u (MPa)	Elongation (%)	Poisson's ratio	Modulus of Elasticity E_s (GPa)
Rectangular (RS)	125 × 75 × 2.8	445.6	482.3	15.4	0.27	205.6
Circular (CS)	135 × 3.0	353.3	422.0	20.1	0.28	207.4

Table 2
Tensile properties of CFRP sheets and adhesive materials.

Material	Thickness (mm)	Ultimate tensile Strength (MPa)	Ultimate Strain (%)	Modulus of Elasticity (GPa)
CFRP (nominal)	0.13	4900	2.1	230.0
CFRP (measured)	0.13	3224	1.8	228.0
Epoxy (nominal)	–	30	0.9	4.5

pons tests (measured) and/or given by the manufacturer (nominal). The thickness of one CFRP sheet (0.13 mm) was measured using a vernier scale.

2.2. Test specimens

Fourteen specimens of CFST beams, including eight rectangular cross-section specimens and six circular cross-section specimens were subjected to pure flexural loads (four-point bending). Generally, the strengthening schemes were achieved by applying the unidirectional CFRP sheets along the bottom-half of the specimens' cross-sections. Fig. 1 shows the details of the strengthening schemes applied to the rectangular and circular specimens, which are presented as well in Tables 3 and 4, respectively. The specimens' designations, RS and CS, refer to the beams' cross-sections, which are rectangular and circular specimens, respectively. Both RS1 and RS2 are the control specimens of the rectangular beams, and CS is the control specimen of the circular beams. The numbers and letter 100P, 75P, and 50P represent the partial-unilateral CFRP strengthening scheme, which is known as the 'partial/U-shaped' scheme (P) applied along a varying percentage of the beams' effective lengths (L_e): 100%, 75%, and 50%, respectively. The last number and letter represent the total number of CFRP layers (for instance, 3L = three layers). Two rectangular beams have been strengthened along their full lengths using two CFRP layers, the orientations of these layers may both be parallel to the beam (RS-100F-2L), representing the full-unilateral strengthening scheme which is known as the 'full' scheme (F). Alternatively, the orientation of the first layer may be parallel to the beam and that of the second layer may be perpendicular to the beam (RS-100C-2L), representing the full-bilateral strengthening scheme which is known as the 'combined' scheme (C). Furthermore, tiny, artificial scratches were made along the bonding surface of one circular beam (CS-50P-2LA) to improve the mechanical bonds that interlocked with the adhesive material. This action was suggested to investigate the effects of the surface's roughness on the bonding strength, specifically for the beam to which a sheet was applied partially along 50% of its length. The total percentages of specimen's surface area that need to be covered with CFRP sheets for each strengthening scheme are clarified in Tables 3 and 4 as well (i.e. 100%, 50%, 37.5% and 25%). The effective specimens' length (L_e) were equal to 1850 mm (support-to-support), and the depth/diameter-to-thickness (D/t) ratios were 44.6 and 45.0 for the rectangular and circular tubes, respectively.

2.3. Specimen preparation

The steel tube specimens were placed upright and covered temporarily on the bottom side with rubber sheets to prevent the water of concrete from leaking out during the casting time. The concrete was cast inside the tubes from the top side in multi layers and vibrated using an electrical vibration device. Twenty-five to 30 days after the casting work, an electrical grinder at low speed was used with a wheel of sandpaper (grit #24) to clean the tubes' surfaces in order to improve the mechanical bonds' interlocking with the epoxy. The ground surfaces in their entirety were cleaned with acetone liquid to ensure there was no rust, paint, and/or any contaminant material before the application of the epoxy material and CFRP sheets. The epoxy was mixed carefully in accordance with the manufacturer's requirements then applied to the specimen surfaces immediately. Then the first layer of unidirectional CFRP sheets was applied parallel to the beam's length. A special ribbed roller was used directly after the application of each CFRP sheet to remove the air void between the layers and to make the adhesive layer as uniformly thick as possible. This procedure was repeated for the specimens strengthened with multiple CFRP layers. For the specimen with a combined strengthening shape, the second CFRP layer was oriented perpendicular to the beam. All specimens were cured at room temperature for a minimum of 10 days.

2.4. Test details

A four-point loading system was adopted in this study to achieve the ultimate bending moment. A manual hydraulic jack with a capacity of 300 kN was used for this purpose as shown in Fig. 2. Three linear variable displacement transducers (LVDTs) were distributed equally underneath the specimens to measure the deflection. Strain gauges were provided to evaluate the tensile stress along the steel tubes and the CFRP sheets at different locations and distances. The test setup with the locations of the LVDTs and strain gauges for the control specimens and those for the strengthened specimens are shown in Figs. 3 and 4, respectively. The load was applied gradually with an increment equivalent to 4–5 kN/min. A computerized data acquisition system was used to log the data obtained from the strain gauges and LVDTs at each step of the specimens' loading.

3. Test results and discussion

3.1. Failure modes

All specimens were loaded beyond their maximum load capacity limit to facilitate understanding of the behaviour of the CFST beams when strengthened with CFRP sheets at the extreme loading stage. In other words, the loading test was continued even after the beams' ultimate failure limits had been achieved. The failure modes of the rectangular and circular beams are presented in

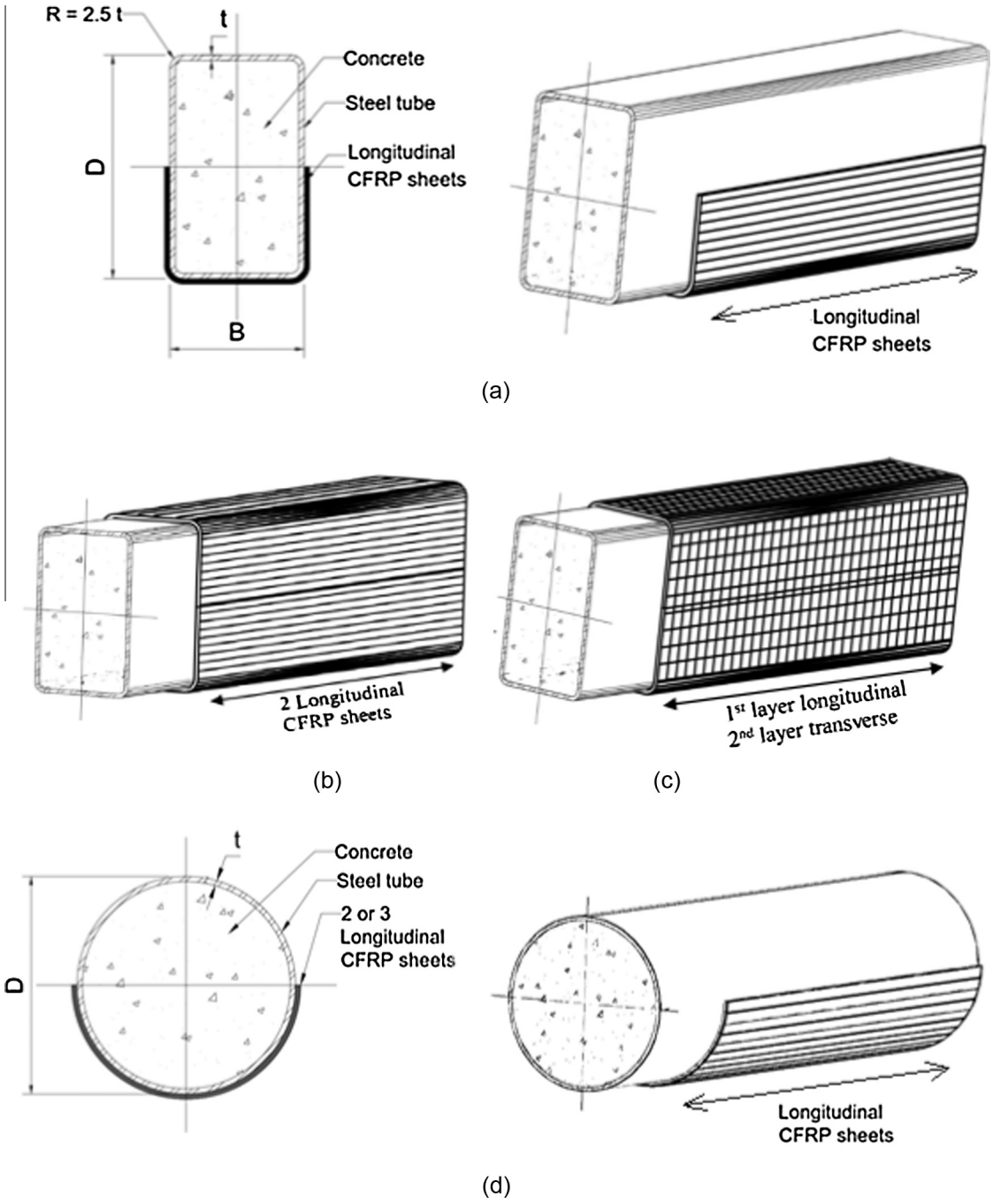

Fig. 1. CFRP strengthening schemes; (a) partial-unilateral (partial) scheme for rectangular specimens, (b) full-unilateral (full) scheme, (c) full-bilateral (combined) scheme, and (d) partial-unilateral (partial) scheme for circular specimens.

Tables 5 and 6, respectively. During the loading stages, no changes were observed in the shapes of the specimens' cross-sections until they achieved their ultimate capacities. The typical outward local buckling failure mode at the tops of the steel tubes (near the loading points) was observed and recorded for all tested specimens, including those strengthened with CFRP sheets. For example, Fig. 5 shows a control (unstrengthened) specimen and strengthened specimens. The major difference between unstrengthened and strengthened specimens was that the latter reached much higher maximum loads before the CFRP sheets ruptured or delaminated. Afterwards, the latter's loads returned to almost the same level as the former's until the outward local failure took place at almost the same deflection value (explained in the next section). Moreover, Fig. 6 shows the curves of some specimens to illustrate the shapes of their deflections at different bending stages which compared to the sine-curve shape. Fig. 7 shows the failure modes of all specimens.

A small crack in the CFRP patch (with cracking sound) was first heard in the pure-tension region (the bottom centre of the specimen) when the strengthened specimens reached about 85–90% of their ultimate load's capacity. Similar failure modes were recorded for all specimens strengthened along 75% and 100% of their lengths. Their CFRP patches were ruptured from the bottom centre once they achieved their ultimate tensile strength due to the high bending stress. Moreover, delamination failure occurred at the edges of the CFRP patches for all the specimens with 50%

Table 3
Designations and strengthening schemes of rectangular CFST specimens.

No.	Specimens' designation	Type of strengthening scheme	% of surface's area covered with CFRP	% of strengthening length (L_{cfrp})	CFRP layers (L)	Strengthening scheme
1	RS1	–	0	0	0	
2	RS2	–	0	0	0	
3	RS-100F-2L	Full	100	100	2	
4	RS-100C-2L	Combined	100	100	2	
5	RS-100P-2L	Partial	50	100	2	
6	RS-100P-3L	Partial	50	100	3	
7	RS-75P-2L	Partial	37.5	75	2	
8	RS-50P-2L	Partial	25	50	2	

Table 4
Designations and strengthening schemes of circular CFST specimens.

No.	Specimens' designation	Type of strengthening scheme	% of Surface's area covered with CFRP	% of strengthening length (L_{cfrp})	CFRP layers (L)	Strengthening scheme
1	CS	–	0	0	0	
2	CS-100P-2L	Partial	50	100	2	
3	CS-100P-3L	Partial	50	100	3	
4	CS-75P-2L	Partial	37.5	75	2	
5	CS-50P-2L	Partial	25	50	2	
6	CS-50P-2LA	Partial	25	50	2	

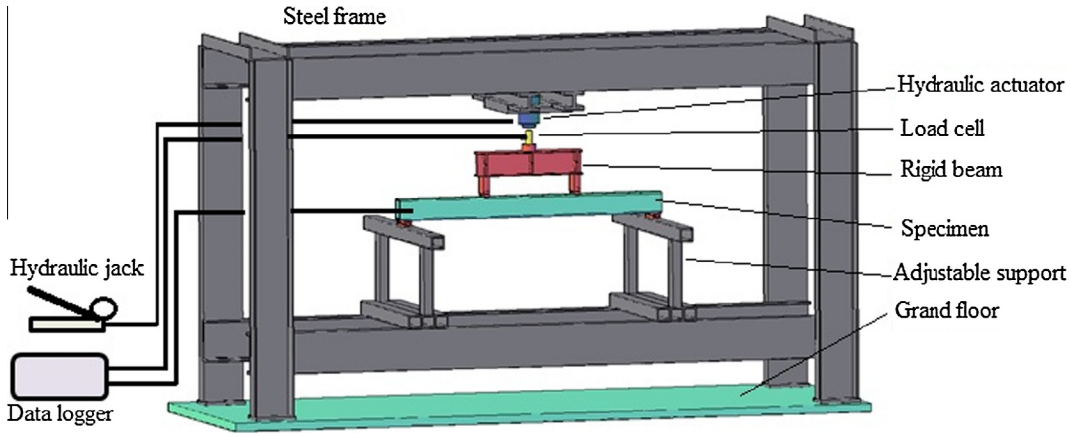

Fig. 2. Test rig system.

strengthening lengths even before the achievement of their ultimate strength. This failure may be attributed to the enormous amount of peeling stress, which occurred along the bonding surfaces between the steel and the CFRP sheets due to the large bending stress at the peeling points. Generally, the value of the peeling stress was proportional to that of the bending stress, reducing gradually with the distance from the beam's mid-span area towards the end supports, similar finding was recorded in [16,17]. Since the CFRP sheets with 50% strengthening lengths were still located within the high-peeling stress zones, delamination failure took place. However, for 75% strengthening lengths, the peeling stress could be overcome by the bonding strength between the CFRP sheets and steel tubes, thus preventing the delamination failure modes from occurring.

As Fig. 8 indicates, the beam with a combined strengthening scheme (RS-100C-2L) showed a gradual CFRP rupture failure (lim-

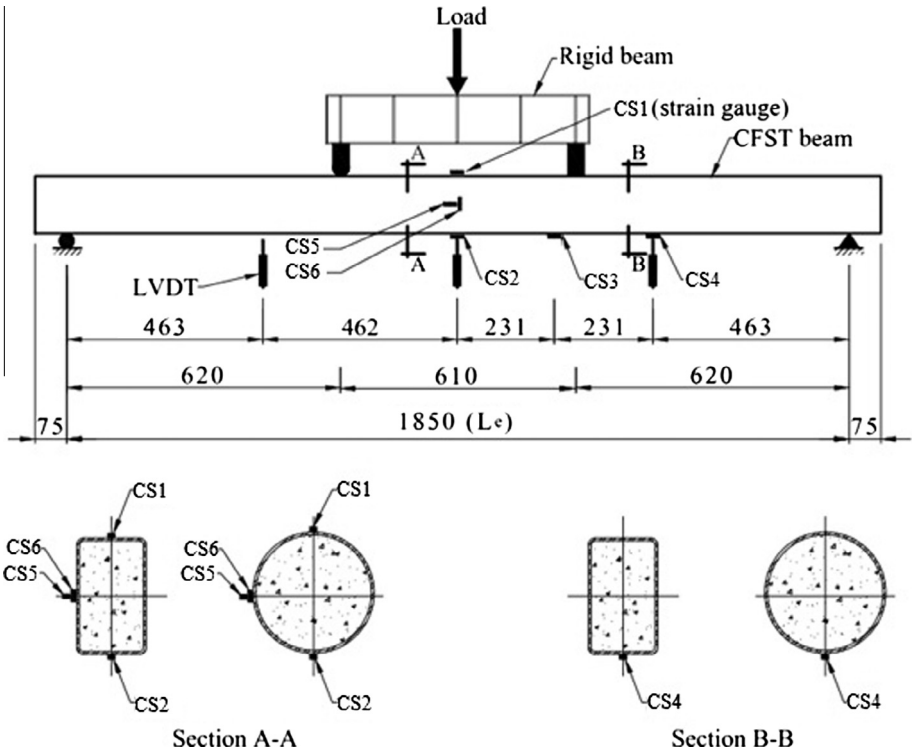

Fig. 3. Test setup of control CFST specimens.

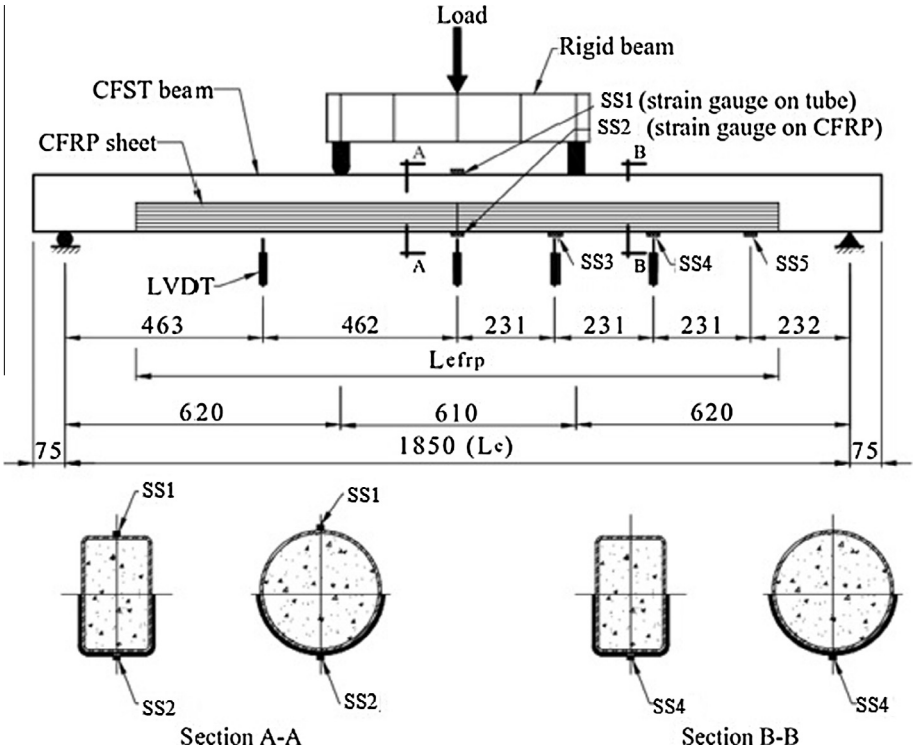

Fig. 4. Test setup of CFST specimens strengthened with CFRP sheets.

ited failure) from the bottom centre unlike the beams with full (RS-100F-2L) and partial (RS-100P-2L) strengthening schemes. This was because the second CFRP layer in the combined scheme, which was oriented perpendicular to the beam, delayed the sudden rupture (longitudinal rupture) that usually occurred with the unidirectional configuration (CFRP layers placed unilaterally in the beam's direction). In all specimens, no slip failure between the concrete core and steel tube was observed where both ends of each specimen were monitored and checked visually during the loading stages.

Table 5
Results of the tested rectangular CFST specimens.

No.	Specimens' designation	M_{ue} (kN. m)	LIR	EA (kN. mm)	K_{ie} (kN. m^2)	K_{se} (kN. m^2)	Failure mode
1	RS1	22.7	–	4228.4	574.2	487.4	Outward local buckling at the top flange of steel tube
2	RS2	23.7	–	4309.0	570.7	480.6	Outward local buckling at the top flange of steel tube
3	RS-100F-2L	29.7	1.28	4654.0	661.7	553.5	Outward local buckling at the top flange of steel tube (preceded by CFRP patch sudden rupture).
4	RS-100C-2L	30.8	1.33	5124.0	625.1	548.9	Outward local buckling at the top flange of steel tube (preceded by CFRP patch gradual rupture).
5	RS-100P-2L	29.3	1.26	4668.2	591.5	515.2	Outward local buckling at the top flange of steel tube (preceded by CFRP patch sudden rupture).
6	RS-100P-3L	32.0	1.38	4993.6	644.6	557.8	Outward local buckling at the top flange of steel tube (preceded by CFRP patch sudden rupture).
7	RS-75P-2L	29.7	1.27	4751.2	617.4	543.8	Outward local buckling at the top flange of steel tube (preceded by CFRP patch sudden rupture).
8	RS-50P-2L	26.1	1.12	4501.7	612.3	535.9	Outward local buckling at the top flange of steel tube (preceded by CFRP patch sudden delamination).

Table 6
Results of the tested circular CFST specimens.

No.	Specimens' designation	M_{ue} (kN. m)	LIR	EA (kN. mm)	K_{ie} (kN. m^2)	K_{se} (kN. m^2)	Failure mode
1	CS	18.5	–	3284.6	624.2	533.8	Outward local buckling at the top flange of steel tube
2	CS-100P-2L	24.3	1.31	4002.9	656.9	579.2	Outward local buckling at the top flange of steel tube (preceded by CFRP patch sudden rupture).
3	CS-100P-3L	26.6	1.44	4361.0	701.4	627.5	Outward local buckling at the top flange of steel tube (preceded by CFRP patch sudden rupture).
4	CS-75P-2L	24.7	1.33	4136.7	667.4	585.4	Outward local buckling at the top flange of steel tube (preceded by CFRP patch sudden rupture).
5	CS-50P-2L	19.9	1.07	3450.1	650.6	563.9	Outward local buckling at the top flange of steel tube (preceded by CFRP patch sudden delamination).
6	CS-50P-2LA	20.5	1.10	3606.0	660.8	569.7	Outward local buckling at the top flange of steel tube (preceded by CFRP patch gradual delamination).

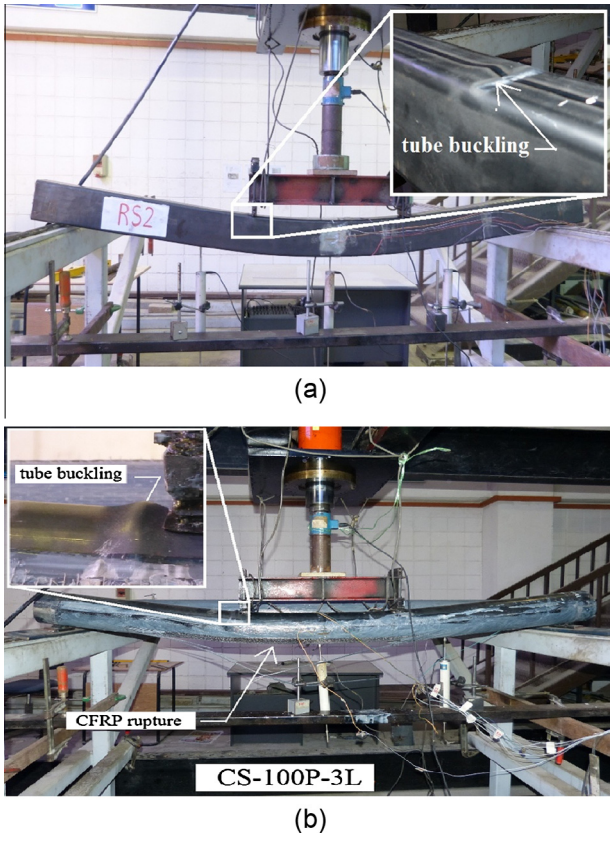

Fig. 5. Typical buckling failure at the top of tubes (at extreme loading stage); (a) RS2 and (b) CS-100P-3L.

3.2. Moment-curvature relationships

Moment (M) versus mid-span curvature (φ) relationships of CFRP-strengthened CFST beams are presented in Figs. 9 and 10 for rectangular and circular cross-sections, respectively. All specimens exhibited elastic behaviour at the initial loading stage followed by inelastic behaviour with gradually decreasing stiffness until the ultimate moment capacity was achieved. Sudden drops in the load curves were observed for the strengthened specimens (in the absence of CFRP patch tensile strength due to the rupture of their fibres or delamination failure). Then, the behaviour of these strengthened specimens became similar to their control specimens until the end of the test (after the influence of CFRP ceased).

Moment-curvature curves of strengthened rectangular specimens using different CFRP strengthening schemes were compared with the average curve obtained from the two control specimens, RS1 and RS2 (see Fig. 9(a)). Fig. 9(b) shows the behaviour of specimens with partial strengthening scheme only, which shows that the specimens strengthened along 75% and 100% of their lengths with 2 CFRP layers (RS-75P-2L and RS-100P-2L) achieved almost the same enhancement. However, the RS-50P-2L specimen (with 50% strengthening length) could not achieve the ultimate tensile strength of its CFRP patch. This was because of the delamination failure, which occurred earlier. In general, increasing the number of CFRP layers increased the load improvement ratio, particularly for specimens that were strengthened along their full lengths. The behaviour of specimens strengthened with the application of 2 CFRP layers along their full lengths but with different strengthening schemes (P, F and C) are compared in Fig. 9(c). In this figure, it is interesting to notice that the partial strengthening scheme (RS-100P-2L) could enhance the capacity of the CFST beam so that it is close to that associated with the application of the full strength-

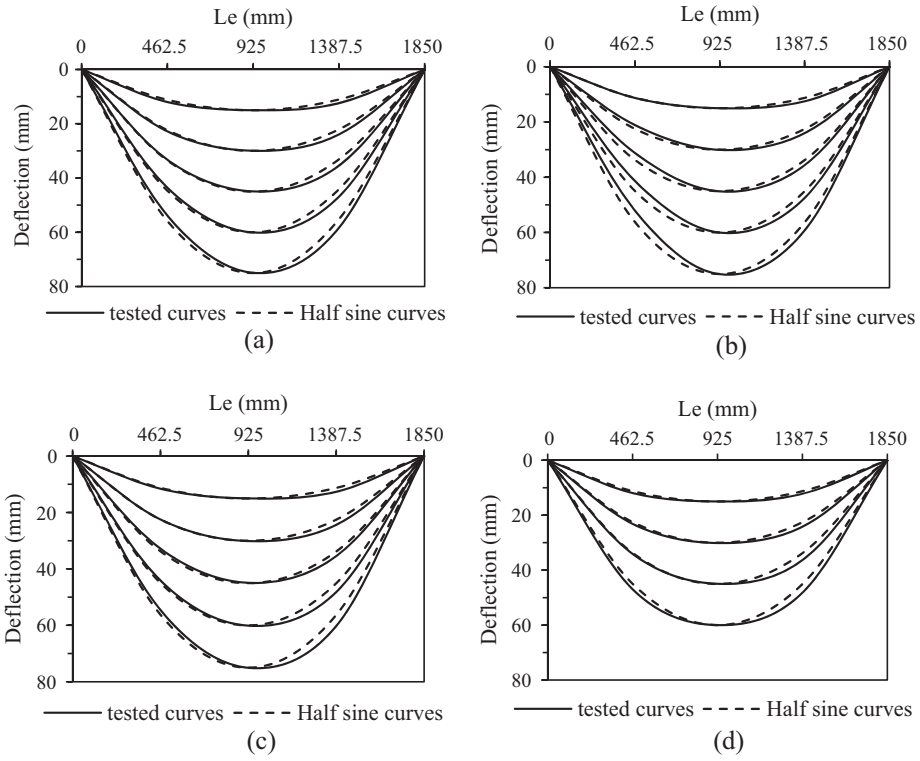

Fig. 6. Deflection shapes along different loading stages; (a) RS2, (b) CS, (c) RS-100P-2L, and (d) CS-100P-3L.

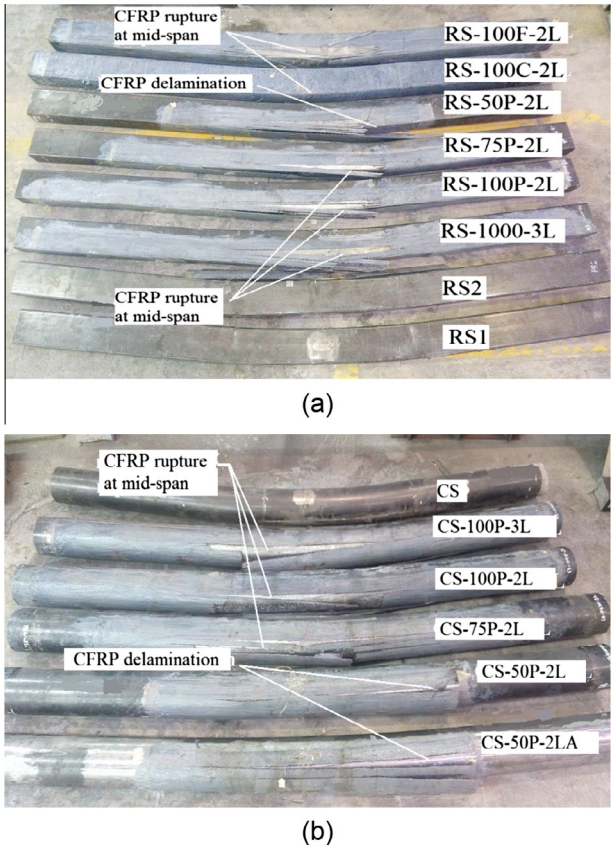

Fig. 7. Failure modes of all tested CFST specimens; (a) rectangular and (b) circular.

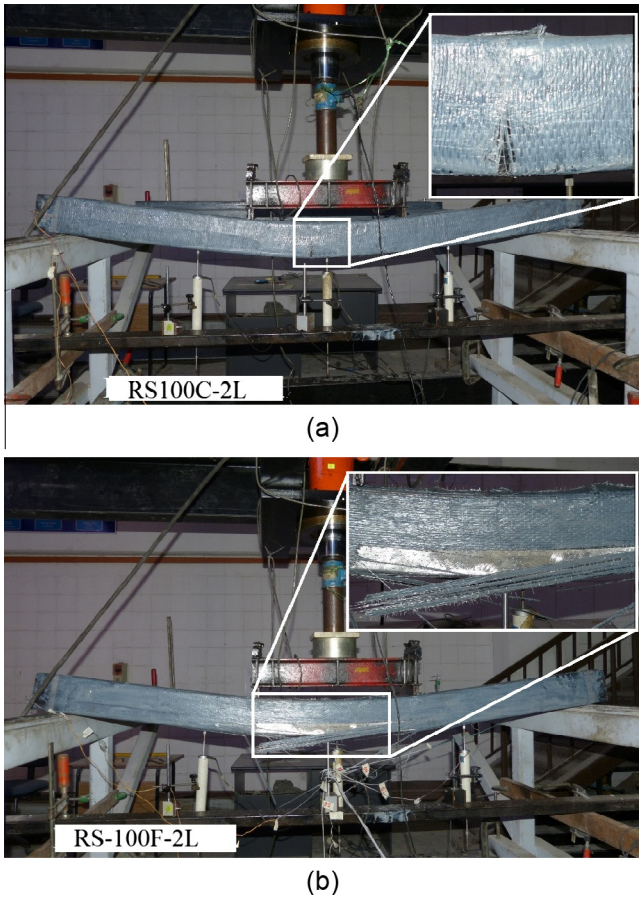

Fig. 8. CFRP failure modes of rectangular specimens; (a) gradual and limited CFRP rupture and (b) sudden and longitudinal CFRP rupture.

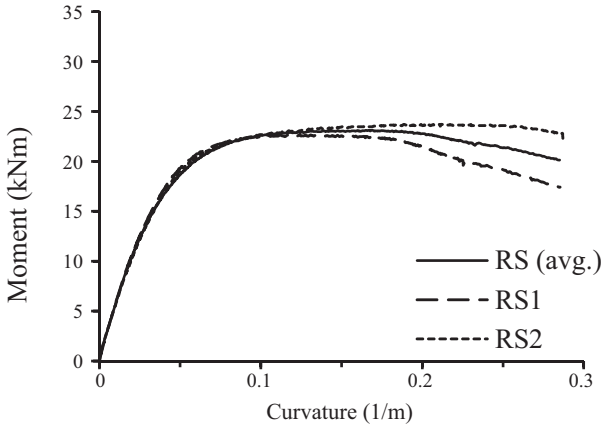

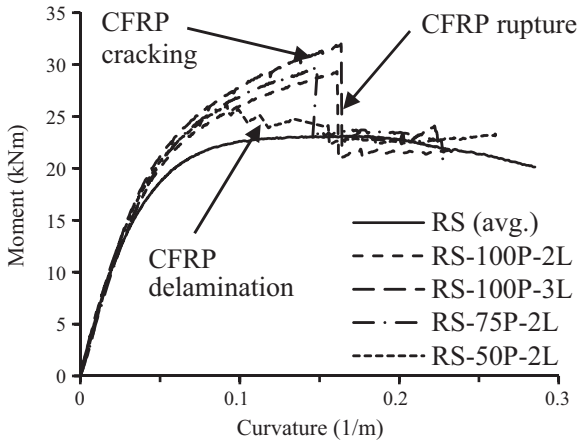

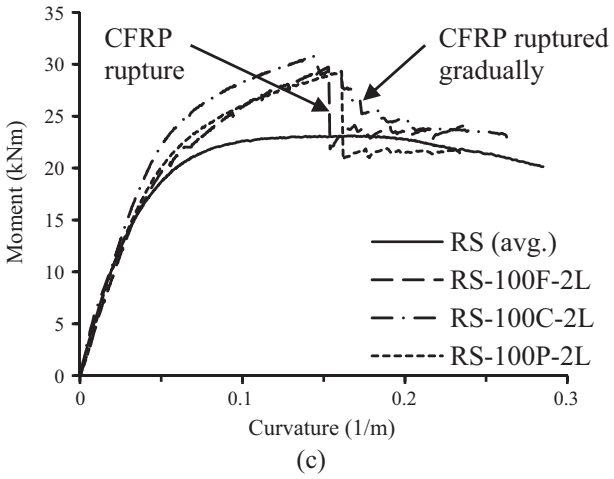

Fig. 9. Moment vs. curvature relationships (at mid-span) of strengthened rectangular CFST specimens; (a) control specimens, (b) specimens with partial scheme only, and (c) specimens with partial, full and combined schemes.

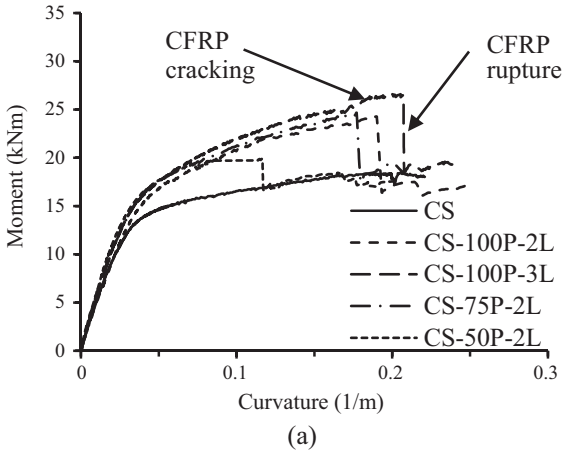

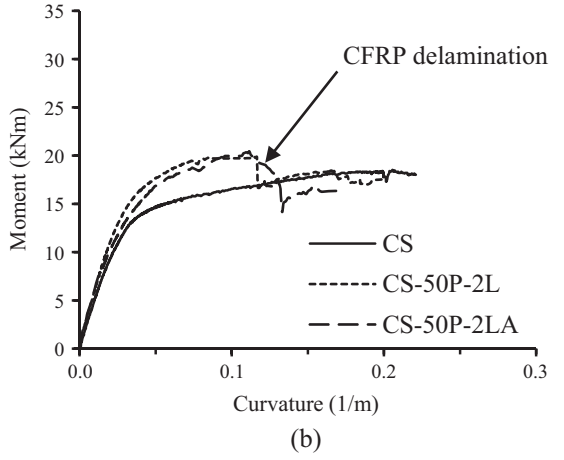

Fig. 10. Moment vs. curvature relationships (at mid-span) of strengthened circular CFST specimens; (a) specimens with partial scheme and (b) effect of artificial scratches.

ening scheme (RS-100F-2L). For both of these specimens, the CFRP sheets that were located in the maximum tension zones (the bottom flange, in the mid-span areas of the specimens) resisted the tensile stress that resulted from bending until they achieved their ultimate tensile strength. However, the CFRP sheets located in the maximum compression zone (top flange, in the mid-span area of the specimen) of specimen RS-100F-2L could not resist the compression stress since CFRP sheets only have the ability to resist tensile stress. Thus, the failure modes and load enhancement ratios for these specimens with partial-unilateral (partial) and full-unilateral (full) strengthening schemes (RS-100P-2L and RS-100F-2L) were almost the same. Ultimately, this behaviour proved that there was not much benefit to strengthening the simply supported CFST beams with CFRP sheets on the top side (compression zone), especially when the sheets were only laid parallel to the beams. Furthermore, the combined scheme (RS-100C-2L) resulted in a lower enhancement in the load capacity of CFST beams than the partial (RS-100P-2L) and full (RS-100F-2L) schemes when the same number of CFRP layers was applied. This was due to its bidirectional strengthening configuration, in which the second CFRP layer delayed the sudden (longitudinal) rupture of the first unidirectional CFRP layer (the layer which was laid parallel to the beam) once it reached its ultimate tensile strength.

Fig. 10 presents the bending moment vs. mid-span curvature curves of the strengthened circular CFST specimens with reference to their control specimen (CS). The behaviour of these circular specimens was almost similar to that of the rectangular specimens with the partial strengthening scheme. As shown in Fig. 10(a), the CS-75P-2L specimen achieved almost the same enhancement as the CS-100P-2L specimen for the same number of CFRP layers (2). The capacity of these beams improved gradually with the increase in the number of CFRP layers. Fig. 10(b) presents a comparison between the moment-curvature curves obtained from the specimens with high and normal surface roughness (CS-50P-2LA and CS-50P-2L). The CS-50P-2LA specimen achieved a slightly

better load enhancement than the CS-50P-2L specimen due to its high surface roughness, which improved the mechanical bond interaction with the adhesive material slightly. This, in turn, slightly delayed the CFRP delamination failure.

The moment vs. strain relationships of the control specimens are presented in Fig. 11, which logically confirms that the tensile strain on the bottom side of the simply supported beams decreased gradually along the distance moved from the mid-span to the support, as the readings of strain gauges CS2, CS3, and CS4 indicated (see Fig. 3 for the strain gauges' numbering and locations). Fig. 12 presents the typical moment vs. strain relationships of CFRP-strengthened specimens up to the CFRP rupture limit (see Fig. 4 for the strain gauges' numbering and locations). These curves also confirm that the tensile strain values along the CFRP patch reduced once they moved away from the beams' mid-span regions to the support ends, where strain gauge SS5 (located at a distance equal to $L_e/8$ from the support) recorded the lowest tensile strain value during the loading stages in comparison to the other strain gauges (SS2, SS3, and SS4). Therefore, using the CFRP sheets with different strengthening schemes to strengthen the CFST beams (rectangular and circular) obviously improved their load capacities, especially in the inelastic range.

3.3. Moment carrying capacity

The ultimate moment capacity (M_{ue}) of all strengthened specimens has been obtained up to the limit of their CFRP sheets was either ruptured or delaminated. The load improvement ratio (LIR) was calculated from the ratio of the M_{ue} value achieved by the strengthened specimen to the ultimate capacity of the control specimen. For the rectangular specimens, the LIR was calculated with reference to the average capacity of the two control specimens (RS1 and RS2). The M_{ue} and LIR values of the rectangular and circular specimens are given in Tables 5 and 6, respectively.

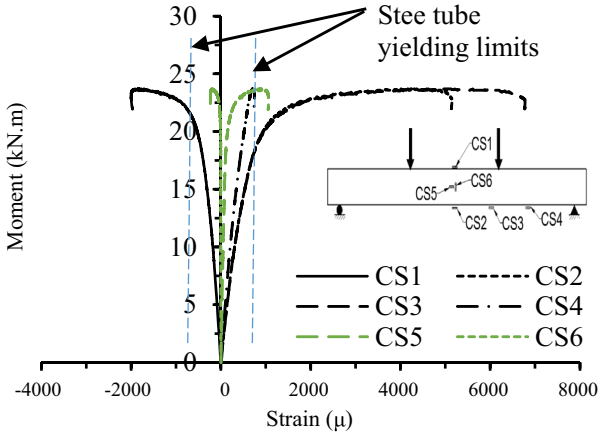

Fig. 11. Typical moment vs. strain relationships of control specimens; (a) RS2 and (b) CS.

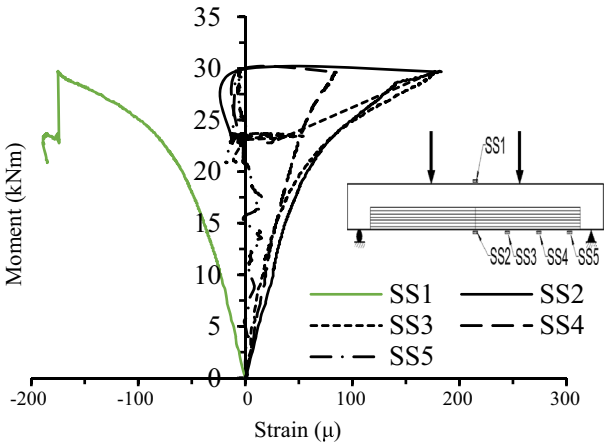

Fig. 12. Moment vs. strain relationships of strengthened specimens (RS-75P-2L).

A comparison of the M_{ue} values of the tested rectangular specimens is presented in Fig. 13. The moment capacity of the specimen with the combined strengthening scheme (RS-100C-2L) was equal to 30.8 kN.m, achieving an LIR of about 1.33. This was higher than the LIR values of the specimens with full and partial schemes, which were 1.28 and 1.26, respectively. In general, increasing the number of CFRP layers led to the gradual improvement of the moment capacity of the strengthened CFST beams. The M_{ue} value of the RS-100P-2L specimen (2 CFRP layers) was equal to 29.3 kN.m. This value increased to 32.0 kN.m with the use of 3 CFRP layers (RS-100P-3L), achieving an LIR of about 1.38. Furthermore, using the partial scheme along 75% of its length with two CFRP layers (RS-75P-2L) raised the specimen's capacity to about +27% above the average capacity of the control specimens. This was very close to that obtained for the RS-100P-2L specimen (+26%) because no CFRP delamination failure occurred in either specimen. The CFRP patches for both specimens were ruptured from the bottom mid-span area once they achieved their ultimate tensile strength. Meanwhile, the 50% strengthening length could only enhance the rectangular beam's capacity by about 12%. Again, this was because of the CFRP delamination failure which occurred earlier.

Fig. 14 presents the values of the ultimate moment capacity related to the circular beams. The highest value was equal to

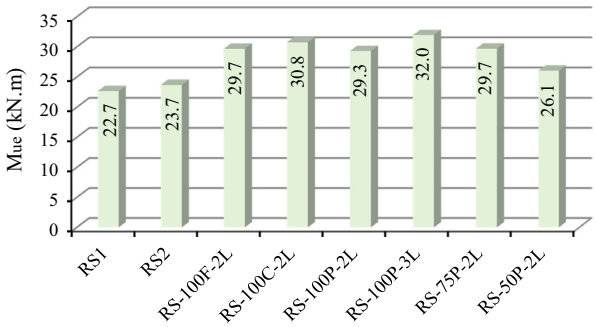

Fig. 13. Ultimate moment capacity (M_{ue}) of rectangular specimens.

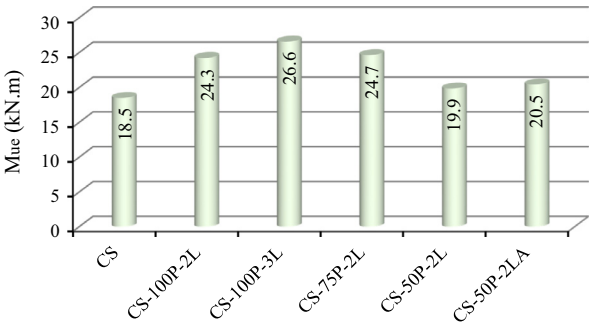

Fig. 14. Ultimate moment capacity (M_{ue}) of circular specimens.

26.59 kN.m, which the specimen strengthened partially with 3 CFRP layers (CS-100P-3L) achieved with an improvement about 44% higher than the capacity of the CS specimen. When the same strengthening scheme was used with 2 CFRP layers, the M_{ue} value was reduced to 24.25 kN.m, achieving an improvement of about 31%. Furthermore, the specimens with 75% and 100% strengthening lengths (CS-75P-2L and CS-100P-2L) achieved very close LIR values of about 1.33 and 1.31, respectively. In comparison, the CS-50P-2L specimen could not achieve an LIR value greater than 1.07 because of the earlier delamination failure, and this value improved a little (1.10) for the CS-50P-2LA specimen. However, the increase in the roughness of the steel surface was not enough to prevent the delamination failure from occurring, because the CFRP sheets were applied along the half-length of the beams and the peeling stress in this zone was still higher than the bonding strength between the CFRP and steel tube, similar failure scenario observed in [16,17]. Though not very significant in this study, the effect of the steel surface's roughness is still in line with the findings reported in previous studies [28–30]. The studies in question concluded that increasing the mechanical bond interaction was dependent on the roughness of the steel surface and the properties of the adhesive (epoxy) material, where increasing the roughness of the steel surface could improve the bonding strength between the two adherent parts. To date, no studies have specifically investigated the mechanical bonding interaction between the CFRP sheets and CFST beams by varying the steel surfaces' roughness. Therefore, in future research, serious attention should be devoted to define the degree of roughness in order to determine the 'effective' roughness that will significantly impact the strengthening characteristics.

3.4. Energy absorption

In the calculation of the area under the curves of load vs. mid-span deflection for the tested composite beams, the energy absorption capacity can be estimated [31]. Fig. 15 shows the procedure which has typically been used to estimate the area under the load-deflection curves for the control and CFRP strengthened specimens. Generally, the strengthened specimens achieved higher load capacities and stiffness values than the control specimens within certain limits before their behaviour went back to being similar to that of the control specimens. Based on the total area under the curves, all the CFST specimens strengthened with CFRP sheets absorbed higher energy than the unstrengthened specimens as Fig. 16 shows with regard to the tested rectangular and circular specimens.

Fig. 16(a) shows that the control specimens, RS1 and RS2, have the lowest energy absorption capacities in comparison to all the CFRP strengthened specimens. These are approximately equal to 4228.4 kN.mm and 4309.0 kN.mm, respectively. The highest value of energy absorption was recorded for the specimens strengthened

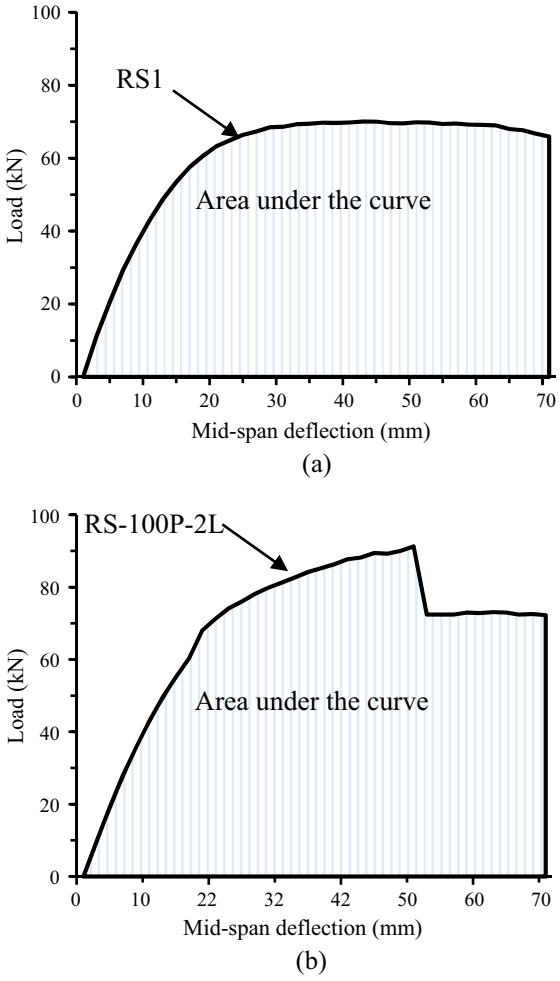

Fig. 15. Typical load vs. mid-span deflection curves for evaluating the absorbed energy, (a) control specimen (RS1) and (b) strengthened specimen (RS-100P-2L).

with 2 CFRP layers using the combined scheme (RS-100C-2L): about 5124.0 kN.mm. Meanwhile, the lowest value for the strengthened specimens, RS-50P-2L, was equal to 4501.7 kN.mm. This was due to the delamination which occurred at the earlier loading stage. However, it was still higher than the values of the control specimens (RS1 and RS2). One of the important findings was that specimens RS-100F-2L, RS-100P-2L, and RS-75P-2L achieved very close energy absorption capacity values: 4654.0, 4668.2, and 4751.2 kN.mm, respectively. As Fig. 16(b) shows, the same findings were recorded for the circular CFST specimens but with different energy absorption values.

3.5. Flexural stiffness

This research also looked into the changes in the flexural stiffness of the CFST beams due to the CFRP sheets. Specimens RS2 and CS-75P-2L were selected as examples to illustrate the typical estimating the flexural stiffness from the moment vs. curvature relationships for the control and strengthened specimens, respectively, as shown in Fig. 17. Both specimens exhibited an initial elastic response followed by inelastic behaviour with gradually decreasing stiffness until the ultimate moment capacity (M_{ue}) was achieved. The moment-curvature curves were used to determine the initial section flexural stiffness (K_{ie}) and the serviceability-level section flexural stiffness (K_{se}) for each tested specimen. The K_{ie} was defined as the secant stiffness corresponding

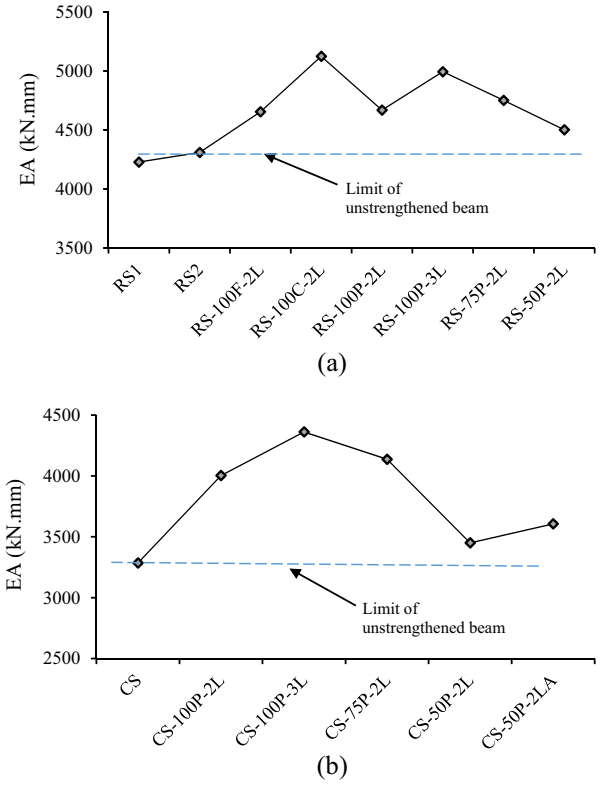

Fig. 16. Energy absorption (EA) capacity; (a) rectangular specimens and (b) circular specimen.

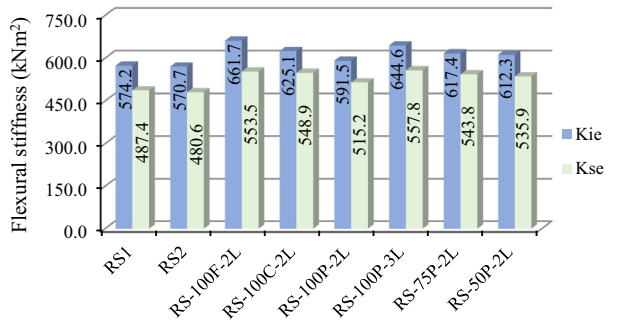

Fig. 18. Flexural stiffness (K_{ie} and K_{se}) of rectangular specimens.

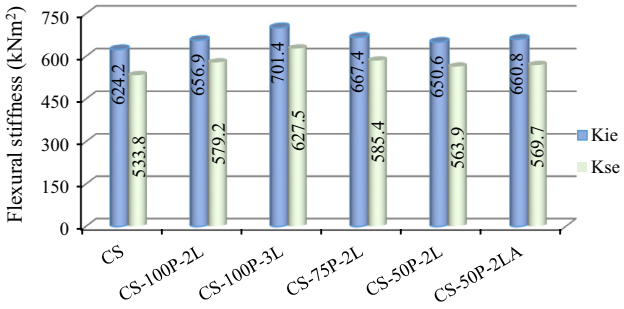

Fig. 19. Flexural stiffness (K_{ie} and K_{se}) of circular specimens.

to the moment of $0.2M_{ue}$, whereas, the K_{se} was defined as the secant stiffness corresponding to the serviceability-level moment of $0.6M_{ue}$ [18,19].

The values of K_{ie} and K_{se} obtained from the experimental tests of the rectangular and circular CFST specimens are listed in Tables 5 and 6, respectively, and presented in Figs. 18 and 19 this section. These figures and tables show that the K_{ie} and K_{se} values increased gradually with the number of CFRP layers. For example, specimen RS2 had K_{ie} and K_{se} values equal to 570.7 kN.m^2 and 480.6 kN.m^2, respectively. These values increased to 644.6 kN.m^2 and 557.8 kN.m^2 when the same specimen was strengthened with 3 CFRP layers (RS-100P-3L), achieving stiffness improvements of about 12.9% and 16.0%, respectively. The same behaviour was observed for the circular specimen, where the CS specimen recorded stiffness values equal to 624.2 kN.m^2 and 533.8 kN.m^2 for the K_{ie} and K_{se}, respectively. These values improved by about 12.3% (701.4 kN.m^2) and 17.5% (627.5 kN.m^2) when strengthened partially with 3 CFRP layers (CS-100P-3L). The difference between the stiffness values of the rectangular and circular specimens was reasonable, even with the same strengthening schemes, and was related to numerous factors, for instance, the difference in their concrete strength, cross-section's moments of inertia, and modulus of elasticity.

The existing code methods, such as AISC (2010) [32], EC4 (2004) [33], BS5400 (1979) [34], and AIJ (1997) [35], are capable of estimating the effective flexural stiffness of CFST members. So far, none of these methods has considered the effects of CFRP materials to play a role in the estimation of the flexural stiffness of the strengthened CFST members. However, the CFRP sheets significantly increased the flexural stiffness of the CFST beams as the current experimental research proves. Therefore, this study suggests predicting the stiffness value of the CFRP part separately then adding it to the relevant formula indicated above. The formulae of the aforementioned methods are listed below:

1. AISC (2010)

$$K_p = E_s \cdot I_s + C1 \cdot E_c \cdot I_c, \quad (1)$$

where, $C1 = 0.6 + 0.2\ (A_s/(A_s + A_c)) \leqslant 0.9$, $E_c = 4733\sqrt{f_c}$

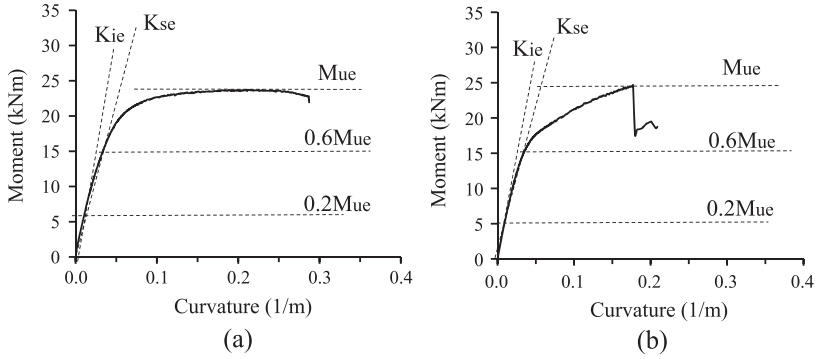

Fig. 17. Typical bending moment-curvature relationships; (a) control specimen (RS2) and (b) strengthened specimen (CS-75P-2L).

2. EC4 (2004)

$$K_p = E_s \cdot I_s + 0.6 \cdot E_c \cdot I_c, \quad (2)$$

where, $E_c = 9500 \times (f_{ck} + 8)^{1/3}$, $f_{ck} = 0.67 \times f_{cu}$

3. BS5400 (1979)

$$K_p = E_s \cdot I_s + E_c \cdot I_c, \quad (3)$$

where, $E_c = 450 \times f_{cu}$

4. AIJ (1997)

$$K_p = E_s \cdot I_s + 0.2 \cdot E_c \cdot I_c, \quad (4)$$

where, $E_c = 21{,}000 \times \sqrt{f_c/19.6}$

In this study, the CFRP patch technique was adopted to represent the multiple CFRP layers including the adhesive layers in between, by transferring them to one equivalent layer, following the same concept that was used in similar studies [16,36]. The moment of inertia of each CFRP patch ($I_{cfrp.patch}$) was calculated from the shape of the strengthening scheme (full/partial) using the total thickness of the CFRP patch ($t_{cfrp.patch}$). The average thickness of each adhesive layer (t_{ad}) was about 0.8–1.0 mm, measured at several places on the strengthened specimens. The CFRP stiffness (K_{cfrp}), total thickness, and equivalent modulus of elasticity for each CFRP patch were evaluated as follows:

$$K_{cfrp} = E_{cfrp.patch} \times I_{cfrp.patch} \quad (5)$$

$$t_{cfrp.patch} = (n \times t_{cfrp.sheet}) + ((n-1) \times t_{ad}) \quad (6)$$

$$E_{cfrp.patch} = \left((n \times t_{cfrp.sheet} \times E_{cfrp.sheet}) + ((n-1) \times t_{ad} \times E_{ad})\right)/t_{cfrp.patch} \quad (7)$$

The total flexural stiffness of the strengthened CFST specimens (K_t) predicted using each method (K_p) plus the stiffness of the CFRP patch (K_{cfrp}) were compared with the initial flexural stiffness and serviceability-level flexural stiffness (K_{ie} and K_{se}) obtained from the current tests, as presented in Tables 7 and 8, respectively. These tables are shows the mean value (MV), the standard deviation, and coefficient of variation (COV) of the ratio of predicted value-to-test value for the different design methods. The results in Table 7 clearly show that the AISC, EC4, and BS5400 methods are conservative for estimating the initial flexural stiffness (K_t/K_{ie}) with MVs of about 1.177, 1.154, and 1.091, respectively, with the COV ranging from 0.056 to 0.065. Meanwhile, the AIJ method achieved a mean value of 0.927 (−7.7%) and a COV of 0.052, which is the best predictor. That's because the AIJ method has used a lower reduction factor (0.2) to estimate the flexural stiffness of the concrete part, compared to the other mentioned methods. Table 8 shows the MV and COV of the ratio of K_t/K_{se} for the same methods. The results in this table show that the AISC, EC4, and BS5400 methods are more conservative for estimating the flexural stiffness at serviceability-level, with MVs of about 1.354, 1.327, and 1.255, respectively, and COVs ranging from 0.056 to 0.064. Also, the AIJ method showed the best predicted values, which were slightly higher than the test results, achieving a mean value of 1.066 (+6.6%) and a COV of 0.050.

Table 7
Comparisons between predicted total flexural stiffness (K_t) and test results of K_{ie}.

No.	Specimens' designation	K_{ie} (kN.m^2)	K_{cfrp} (kN.m^2)	AISC (2010)		EC4 (2004)		BS5400 (1979)		AIJ (1997)	
				K_t (kN.m^2)	K_t/K_{ie}	K_t (kN.m^2)	K_t/K_{ie}	K_t (kN.m^2)	K_t/K_{ie}	K_t (kN.m^2)	K_t/K_{ie}
1	RS1	574.20	0.0	655.1	1.141	636.1	1.108	603.2	1.051	510.6	0.889
2	RS2	570.73	0.0	655.1	1.148	636.1	1.115	603.2	1.057	510.6	0.895
3	RS-100F-2L	661.70	59.6	714.7	1.080	695.7	1.051	662.8	1.000	570.2	0.862
4	RS-100C-2L	625.09	59.6	714.7	1.143	695.7	1.113	662.8	1.060	570.2	0.912
5	RS-100P-2L	591.48	29.8	684.9	1.158	665.9	1.126	633.0	1.070	540.4	0.914
6	RS-100P-3L	644.59	46.9	702.1	1.089	683.0	1.060	650.1	1.009	557.5	0.865
7	RS-75P-2L	617.38	29.8	684.9	1.109	665.9	1.079	633.0	1.025	540.4	0.875
8	CS	624.17	0.0	805.0	1.290	798.5	1.279	747.3	1.197	625.3	1.002
9	CS-100P-2L	656.88	31.4	836.4	1.273	829.9	1.263	778.7	1.185	656.7	1.000
10	CS-100P-3L	701.41	49.2	854.2	1.218	847.7	1.209	796.5	1.136	674.5	0.962
11	CS-75P-2L	667.37	31.4	836.4	1.253	829.9	1.244	778.7	1.167	656.7	0.984
		Mean value (MV)			1.177		1.154		1.091		0.927
		Standard deviation			0.066		0.075		0.064		0.048
		C.O.V			0.056		0.065		0.059		0.052

Table 8
Comparisons between predicted total flexural stiffness (K_t) and test results of K_{se}.

No.	Specimens' designation	K_{se} (kN.m^2)	K_{cfrp} (kN.m^2)	AISC (2010)		EC4 (2004)		BS5400 (1979)		AIJ (1997)	
				K_t (kN.m^2)	K_t/K_{se}	K_t (kN.m^2)	K_t/K_{se}	K_t (kN.m^2)	K_t/K_{se}	K_t (kN.m^2)	K_t/K_{se}
1	RS1	487.39	0.0	655.1	1.344	636.1	1.108	603.2	1.238	510.6	1.048
2	RS2	480.62	0.0	655.1	1.363	636.1	1.115	603.2	1.255	510.6	1.062
3	RS-100F-2L	553.23	59.6	714.7	1.292	695.7	1.098	662.8	1.198	570.2	1.031
4	RS-100C-2L	548.92	59.6	714.7	1.302	695.7	1.113	662.8	1.207	570.2	1.039
5	RS-100P-2L	515.17	29.8	684.9	1.329	665.9	1.126	633.0	1.229	540.4	1.049
6	RS-100P-3L	557.85	46.9	702.1	1.259	683.0	1.060	650.1	1.165	557.5	0.999
7	RS-75P-2L	543.84	29.8	684.9	1.259	665.9	1.079	633.0	1.164	540.4	0.994
8	CS	533.84	0.0	805.0	1.508	798.5	1.496	747.3	1.400	625.3	1.171
9	CS-100P-2L	579.17	31.4	836.4	1.444	829.9	1.433	778.7	1.345	656.7	1.134
10	CS-100P-3L	627.52	49.2	854.2	1.361	847.7	1.351	796.5	1.269	674.5	1.075
11	CS-75P-2L	585.43	31.4	836.4	1.429	829.9	1.418	778.7	1.330	656.7	1.122
		Mean value (MV)			1.354		1.327		1.255		1.066
		Standard deviation			0.076		0.085		0.072		0.053
		C.O.V			0.056		0.064		0.058		0.050

4. Conclusions

This paper highlights an experimental test study concerning rectangular and circular CFST beams strengthened with unidirectional CFRP sheets using different strengthening schemes and varied layers and lengths. The conclusions of the results can be summarized as follows:

- The moment-carrying capacity of the strengthened CFST beams increased with the number of CFRP layers in principle. For example, the moment capacities of the tested rectangular and circular CFST beams which were strengthened partially (U-shaped) with 2 CFRP layers improved by about 28% and 33%, respectively, compared to the capacity of their control beam. These capacities increased by about 38% and 44% when 3 CFRP layers were used.
- The full-bilateral (combined) CFRP strengthening scheme resulted in the slight improvement in the strength of the CFST beams in comparison to those strengthened with the full-unilateral (full) and partial-unilateral (partial) schemes, particularly when they all used the same number of CFRP layers. This was because the second CFRP layer, which was oriented perpendicular to the beam's direction, delayed the longitudinal rupture, which usually occurred in the first layer (the layer oriented parallel to the beam's direction) once it reached its ultimate tensile strength.
- The rectangular CFST beams strengthened partially along 75% and 100% of their lengths (RS-75P-2L and RS-100P-2L) and the one with full strengthening scheme along 100% of its length (RS-100F-2L) achieved almost the same failure modes and load-improvement ratios (1.26–1.28) as the control beam. That meant that if the beam was partially strengthened over only 37.5% of its surface area (RS-75P-2L) with the unidirectional CFRP sheets, it would have achieved almost the same load enhancement as one that was fully strengthened over 100% of its surface area (RS-100F-2L). In other words, the saving in CFRP sheet's amount would have been about 62.5%, and the same load improvement ratio would still have been achieved.
- CFRP delamination failure occurred for all CFST beams which were partially strengthened along 50% of their lengths (RS-50P-2L and CS-50P-2L). However, increasing the steel surface roughness for this type of strengthening scheme (CS-50P-2LA) was not enough to prevent the CFRP delamination failure from occurring. This was because an enormous amount of peeling stress was still effective in the half-length zone of the beam. Therefore, in future research, serious attention shall be devoted to defining the degree of roughness in order to discover the 'effective' roughness that will significantly impact the strengthening characteristics, particularly when using partial CFRP strengthening schemes.
- The CFRP sheets improved the capability of the CFST beams to absorb more energy where the type of strengthening scheme and/or number of CFRP layers had major influences on their energy absorption capacities. For example, the energy absorption capacity of the circular CFST beam that was partially strengthened with 2 CFRP layers along 100% of its length increased by about +21.8%, compared to the control beam. Then, this value increased more by about +32.7% when 3 CFRP layers were used.
- The flexural stiffness of the CFST beams increased gradually with the number of CFRP layers. It was observed that the CFRP sheets increased the beam's stiffness in the inelastic range to a greater extent than they did its stiffness in the elastic range. For example, strengthening the rectangular beam partially (U-shaped) with 2 layers of CFRP sheets increased its flexural stiffness by about 12.9% and 16.0% at the initial and serviceability stages, respectively.
- In general, the flexural stiffness predicted from different existing methods (such as AISC, EC4, BS5400) in addition to the stiffness effects of CFRP sheets overestimated the experimental results, while, the AIJ method better predict the experimental values, where it was achieved MV about 0.927 with COV of 0.052, for stiffness values at initial level, and MV about 1.066 with COV of 0.050 for stiffness values at serviceability-level.

Acknowledgments

The authors gratefully acknowledge the financial support for this research provided by the Universiti Kebangsaan Malaysia (UKM) – Malaysia, with grant No. (DLP-2014-001). Special thanks to Mr. Mohd Rizal and Miss Malini for their great assistance in conducting the experimental work at the structural laboratory of UKM.

References

[1] Nakamura S-i, Momiyama Y, Hosaka T, Homma K. New technologies of steel/concrete composite bridges. J Constr Steel Res 2002;58(1):99–130.
[2] Kang J-Y, Choi E-S, Chin W-J, Lee J-W. Flexural behavior of concrete-filled steel tube members and its application. Int J Steel Struct 2007;7:319–24.
[3] Elchalakani M, Zhao XL. Concrete-filled cold-formed circular steel tubes subjected to variable amplitude cyclic pure bending. Eng Struct 2008;30(2):287–99.
[4] Bambach MR, Jama H, Zhao XL, Grzebieta RH. Hollow and concrete filled steel hollow sections under transverse impact loads. Eng Struct 2008;30(10):2859–70.
[5] Tao Z, Han L-H, Wang L-L. Compressive and flexural behaviour of CFRP-repaired concrete-filled steel tubes after exposure to fire. J Constr Steel Res 2007;63(8):1116–26.
[6] Zhao X-L, Zhang L. State-of-the-art review on FRP strengthened steel structures. Eng Struct 2007;29(8):1808–23.
[7] Ganesh Prabhu G, Sundarraja MC. Behaviour of concrete filled steel tubular (CFST) short columns externally reinforced using CFRP strips composite. Constr Build Mater 2013;47:1362–71.
[8] Tao Z, Han L-H. Behaviour of fire-exposed concrete-filled steel tubular beam columns repaired with CFRP wraps. Thin-Walled Struct 2007;45(1):63–76.
[9] Park JW, Choi SM. Structural behavior of CFRP strengthened concrete-filled steel tubes columns under axial compression loads. Steel Compos Struct 2013;14(5):453–72.
[10] Dong JF, Wang QY, Guan ZW. Structural behaviour of recycled aggregate concrete filled steel tube columns strengthened by CFRP. Eng Struct 2013;48:532–42.
[11] Park J, Hong Y, Hong G, Kim J, Choi S. Design formulas of concrete filled circular steel tubes reinforced by carbon fiber reinforced plastic sheets. Procedia Eng 2011;14:2916–22.
[12] Hu Y, Yu T, Teng J. FRP-confined circular concrete-filled thin steel tubes under axial compression. J Compos Constr 2011;15(5):850–60.
[13] Liu L, Lu Y. Axial bearing capacity of short FRP confined concrete-filled steel tubular columns. J Wuhan Univ Technol-Mater Sci Ed 2010;25(3):454–8.
[14] Tao Z, Han L-H, Zhuang J-P. Axial loading behavior of CFRP strengthened concrete-filled steel tubular stub columns. Adv Struct Eng 2007;10(1):37–46.
[15] Teng JG, Hu YM, Yu T. Stress–strain model for concrete in FRP-confined steel tubular columns. Eng Struct 2013;49:156–67.
[16] Al Zand AW, Badaruzzaman WHW, Mutalib AA, Qahtan AH. Finite element analysis of square CFST beam strengthened by CFRP composite material. Thin-Walled Struct 2015;96:348–58.
[17] Sundarraja MC, Prabhu GG. Flexural behaviour of CFST members strengthened using CFRP composites. Steel Compos Struct 2013;15(6):623–43.
[18] Wang QL, Shao YB. Flexural performance of circular concrete filled CFRP-steel tubes. Adv Steel Constr 2015;11(2):127–49.
[19] Wang QL, Li J, Shao YB, Zhao WJ. Flexural performances of square concrete filled CFRP-steel tubes (S-CF-CFRP-ST). Adv Struct Eng 2015;18(8):1319–44.
[20] Wang Z-B, Yu Q, Tao Z. Behaviour of CFRP externally-reinforced circular CFST members under combined tension and bending. J Constr Steel Res 2015;106:122–37.
[21] Elchalakani M. CFRP strengthening and rehabilitation of degraded steel welded RHS beams under combined bending and bearing. Thin-Walled Struct 2014;77:86–108.
[22] Haedir J, Bambach MR, Zhao XL, Grzebieta RH. Strength of circular hollow sections (CHS) tubular beams externally reinforced by carbon FRP sheets in pure bending. Thin-Walled Struct 2009;47(10):1136–47.
[23] Miller TC, Chajes MJ, Mertz DR, Hastings JN. Strengthening of a steel bridge girder using CFRP plates. J Bridge Eng 2001;6(6):514–22.

[24] Kim YJ, Harries KA. Fatigue behavior of damaged steel beams repaired with CFRP strips. Eng Struct 2011;33(5):1491–502.
[25] Colombi P, Fava G. Experimental study on the fatigue behaviour of cracked steel beams repaired with CFRP plates. Eng Fract Mech 2015;145:128–42.
[26] ASTM-E8/E8M. Standard test methods for tension testing of metallic materials. West Conshohocken (USA); 2009.
[27] ASTM-D3039. Standard test method for tensile properties of polymer matrix composite material. In: Annual book of ASTM standards. West Conshohocken (PA): American Society for Testing and Materials; 2000.
[28] Fernando ND. Bond behaviour and debonding failures in CFRP-strengthened steel members [Ph.D. thesis]. Civil and Structural Department, Hong Kong Polytechnic University; 2010. p. 343.
[29] Packham DE. Surface energy, surface topography and adhesion. Int J Adhes Adhes 2003;23(6):437–48.
[30] Baldan A. Adhesively-bonded joints and repairs in metallic alloys, polymers and composite materials: adhesives, adhesion theories and surface pretreatment. J Mater Sci 2004;39(1):1–49.
[31] Arivalagan, Kandasamy. Energy absorption capacity of composite beams. J Eng Sci Technol Rev 2009;2(1):145–50.
[32] AISC. Specification for structural steel buildings. Chicago, IL: AISC; 2010.
[33] EC4. European Committee for Standardization. Design of composite steel and concrete structures – Part 1. 1: General rules and rules for buildings. Brussels; 2004.
[34] BS5400. British Standard Institute: Part 5, concrete and composite bridges; 1979.
[35] AIJ. Architectural Institute of Japan (AIJ). Recommendations for design and construction of concrete filled steel tubular structures; 1997.
[36] Al-Zand AW, Badaruzzaman WHW, Mutalib AA, Hilo SJ. Modelling the delamination failure along the CFRP-CFST beam interaction surface using different finite element techniques. J Eng Sci Technol 2017;12(2):1–15.